doi:10.1111/j.1558-5646.2010.01133.x

MODULARITY AND SCALING IN FAST MOVEMENTS: POWER AMPLIFICATION IN MANTIS SHRIMP

Thomas Claverie,[1,2] Elliot Chan,[3] and Sheila N. Patek[1]

[1]*Department of Biology, University of Massachusetts, Amherst, Massachusetts 01003*

[2]*E-mail: claverie@bio.umass.edu*

[3]*Department of Integrative Biology, University of California, Berkeley, California 94720*

Received June 10, 2010
Accepted August 30, 2010

Extremely fast animal actions are accomplished with mechanisms that reduce the duration of movement. This process is known as power amplification. Although many studies have examined the morphology and performance of power-amplified systems, little is known about their development and evolution. Here, we examine scaling and modularity in the powerful predatory appendages of a mantis shrimp, *Gonodactylaceus falcatus* (Crustacea, Stomatopoda). We propose that power-amplified systems can be divided into three units: an engine (e.g., muscle), an amplifier (e.g., spring), and a tool (e.g., hammer). We tested whether these units are developmentally independent using geometric morphometric techniques that quantitatively compare shapes. Additionally, we tested whether shape and several mechanical features are correlated with size and sex. We found that the morphological regions that represent the engine, amplifier, and tool belong to independent developmental modules. In both sexes, body size was positively correlated with the size of each region. Shape, however, changed allometrically with appendage size only in the amplifier (both sexes) and tool (males). These morphological changes were correlated with strike force and spring force (amplifier), but not spring stiffness (amplifier). Overall, the results indicate that each functional unit belongs to different developmental modules in a power-amplified system, potentially allowing independent evolution of the engine, amplifier, and tool.

KEY WORDS: **Geometric morphometrics, raptorial appendage shape, scaling, Stomatopoda, strike force.**

Fast biological movements fascinate biologists for their remarkable biomechanical designs and behavioral feats. Studies of these systems have formed the foundation of a field focused on power amplification—the mechanism by which organisms reduce the time to perform a movement (Alexander and Bennet-Clark 1977; Alexander 1983); however, little attention has been given to the evolution of their morphology. Studies of the modular organization of organisms have brought fundamental insights to the understanding of the development and evolution of traits and organs (Wagner 1996; Wagner and Altenberg 1996; Schlosser 2002; West-Eberhard 2003). Here, we integrate these two fields by examining three functional units of a power-amplified system and testing whether these units belong to independent developmental modules. Knowing how the different functional units of power amplification systems match developmental units both enhances understanding of ontogenetic and scaling studies (West-Eberhard 2003) and has the potential to yield important and novel insights into the evolutionary history of power-amplified structures.

Fast movements are achieved through the use of springs, linkages, levers, and latches (Gronenberg et al. 1993; Gronenberg 1996; Roberts et al. 1997; de Groot and van Leeuwen 2004; Edwards et al. 2005; Deban et al. 2007; Williams et al. 2007; Van Wassenbergh et al. 2008). Power amplification systems are fantastically diverse both structurally and taxonomically, yet most can be described with a simple model consisting of three functional units: an "engine" (e.g., muscle) that slowly loads an "amplifier" (e.g., spring) which rapidly moves a "tool" (e.g., appendage) (Fig. 1). Whether the power-amplified

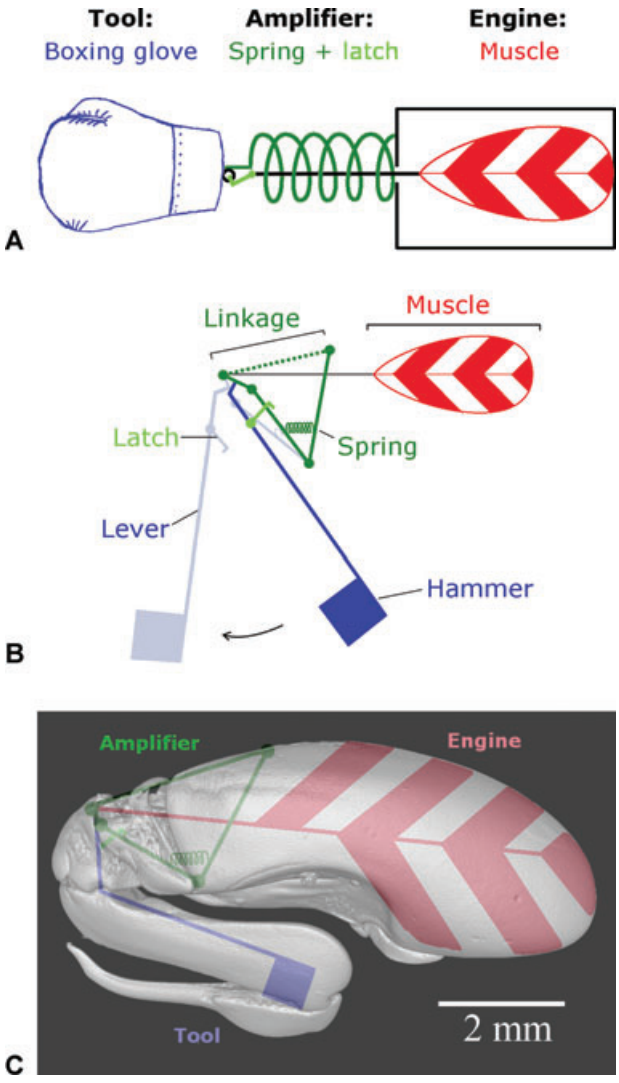

Figure 1. **A power amplification system typically consists of three units: an engine, amplifier, and tool. (A) A theoretical drawing of a muscle-powered punching glove shows that the muscle contraction (engine) loads a spring and latch system (amplifier) which then releases and powers the punching glove (tool). (B) These same units are present in the mantis shrimp's raptorial appendage. A large extensor muscle (engine) loads a spring (amplifier) and linkage system controlled by a latch that releases the hammer (tool) over a short time period. (C) The engine, amplifier, and tool are overlaid on a micro-CT image of a *G. falcatus* appendage (dorsal is toward the top of the page; distal is to the left).**

structure is the leg of a jumping locust, the tongue of a chameleon or the mandibles of trap-jaw ants, these three functional units are always present (Rothschild et al. 1972; Bennet-Clark 1975; Gronenberg and Ehmer 1996; Herrel et al. 2000; de Groot and van Leeuwen 2004). By using this simple yet robust model, it is possible to examine the whole power-amplified system in relation to the variation and interconnectedness of each of its parts. Thus, this model approach offers a foundational framework for understanding the flexibility and limitations on both individual-level variation and cross-species variation in power-amplified systems.

Understanding whether the engine, amplifier, and tool can be modified as independent, modular units or as developmentally interconnected regions requires operational definitions of two terms—behavioral "functional modularity" and morphological "developmental modularity." A "functional module" is defined as a single structure or group of structures that are used for a common behavior (Moss 1968; Moss and Salentijn 1969; Klingenberg 2008). For example, in mammal mandibles, the anterior region that holds the teeth is the functional module associated with food processing. The posterior half of the mandible corresponds to the region where muscles are inserted and represent the functional module associated with mastication movement (Moss 1968; Atchley and Hall 1991; Cheverud et al. 1991; Klingenberg et al. 2003). In contrast, a "developmental module" is defined as a single structure or group of structures that share common cellular and molecular mechanisms during development (Atchley and Hall 1991; Wagner and Altenberg 1996; Bolker 2000; Klingenberg 2008). Developmental modularity is detected through shared or independent morphological variation. For example, a study of bumblebee wings indicated that the variation in forewing morphology between left and right sides or among specimens was internally congruent, but different from the variation in the hind-wing morphology. This result demonstrated that each pair of wings belongs to different developmental modules, which is consistent with the fact that fore- and hind-wings develop from different imaginal discs (Klingenberg et al. 2001).

In the context of power-amplified systems, the engine, amplifier, and tool are different functional modules, because they each perform a different task at a different time and at different time scales. To detect whether these functional modules are also developmental modules requires examining the morphological variation underlying each functional module. Thus, morphological variation of the engine, amplifier, and tool serves as a proxy for developmental integration of these parts. Developmental modularity suggests a greater likelihood of independent evolution of the units and "fine-tuning" to their function at a given ontogenetic stage or environment (Wagner 1996; Waxman and Peck 1998; Schlosser 2002; West-Eberhard 2003; Otto 2004; Snell-Rood et al. 2010). Conversely, if the engine, amplifier, and tool share a single developmental program, evolutionary variation among the parts may be limited to a narrower range.

We focused on the raptorial appendage of a mantis shrimp, *Gonodactylaceus falcatus* (Stomatopoda, Crustacea) to study scaling and modularity of a power-amplified system. This species hammers hard-shelled prey (Fig. 2) (Pit and Southgate 2003) and uses the typical stomatopod engine and amplifier to achieve extremely rapid, power-amplified strikes (Burrows 1969; Patek et al. 2004, 2007). Specifically, a large extensor muscle (the

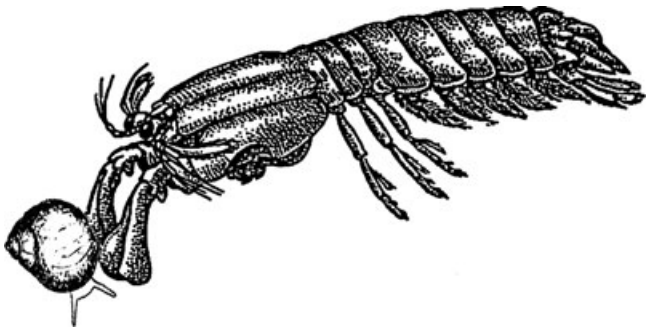

Figure 2. Many mantis shrimp species smash hard-shelled prey with their hammer-shaped raptorial appendages. Drawing modified from Caldwell and Dingle (1976).

engine) gradually compresses a spring (the amplifier) in preparation for a strike, whereas flexor muscles engage latches to prevent movement (Burrows 1969; Burrows and Hoyle 1972; Patek et al. 2004, 2007; Zack et al. 2009). When ready to strike, the latches are released and the stored elastic energy is rapidly delivered to a linkage and lever system that yields a rapid strike (Patek et al. 2004, 2007; Patek and Caldwell 2005; Zack et al. 2009). At the end of the lever, stomatopod appendages possess either a rounded and strongly calcified hammer (the tool), as in *G. falcatus,* or numerous sharp serrated teeth to smash or spear prey (Caldwell and Dingle 1976; Ahyong 2001; Patek and Caldwell 2005; Patek et al. 2007).

An interesting feature of this system is that the engine, amplifier, and tool are mechanically linked, but spatially distinct on the appendage (Fig. 1), which allows for studies of scaling and modularity in these regions. Two studies have examined scaling in mantis shrimp raptorial appendages. One study of *G. falcatus* examined the scaling of the amplifier, finding that body size was positively correlated with elastic energy storage, but not with spring stiffness (Zack et al. 2009). A study of *Odontodactylus scyllarus* found a positive correlation between tool size and force generation (Patek and Caldwell 2005). Finally, although developmental modularity has not yet been studied in stomatopod crustaceans, developmental studies of crustaceans and other arthropods have shown that the morphology and segmentation of appendages is spatially and temporally controlled by a network of regulatory genes that permit a modular development of these structures (Pangamiban et al. 1995; Browne and Patel 2000; Williams and Nagy 2001).

Toward the broader goal of understanding the developmental and evolutionary underpinnings of power amplification, we used geometric morphometric techniques to examine scaling, shape variation, sexual dimorphism and developmental modularity in the engine, amplifier, and tool of *G. falcatus*. For the amplifier, we examined the correlation between mechanical behavior of the spring (stiffness and elastic energy storage) in relation to the size and shape of the structure. We also tested whether variation in these units were correlated with strike force. It is important to note that this study applies analyses of shape to a biomechanical system, but does not incorporate biomechanical analyses to computationally determine the biomechanical consequences of these differences in shape. Thus, this is primarily a study of two-dimensional (2D) shape variation with the goal of providing a first, foundational study integrating geometric morphometric techniques with the fundamental principles of power amplification.

In the course of this study, we addressed the three following questions: (1) Do the units of a power amplification system scale similarly or does each unit follow its own mechanical scaling rules? (2) How does shape variation relate to the mechanics of the system? (3) Do the engine, amplifier, and tool exhibit shape variation indicative of developmental modularity and might this contribute to the diversity of tools across mantis shrimp species?

Materials and Methods

COLLECTION AND MEASUREMENT OF SPECIMENS

Gonodactylaceus falcatus specimens were collected at Oahu, Hawaii in June 2008. Only animals with intact appendages were returned to the laboratory at the University of California, Berkeley for measurement. Body length was measured for each individual (digital electronic vernier caliper, Absolute coolant proof IP 67, ±0.02 mm, Mitutoyo Corp., Kawasaki, Japan). A total of 56 animals (34 females and 22 males) with body lengths ranging from 20 to 60 mm were collected and euthanized by freezing.

To assist in visualizing the component parts of the appendage (Fig. 3), a three-dimensional (3D) representation of the appendage was obtained from micro-Computed Tomography (micro-CT) scans (model HMXST225, X-Tek, Tyngsboro Business Park, MA) and 3D reconstruction software (VGStudio Max version 2, Volume Graphics GmbH, Heidelberg, Germany). A freshly frozen individual of *G. falcatus* was scanned with 0.0086 mm × 0.0086 mm × 0.0086 mm voxel size. Isosurface rendering was used to show the surface conformation of the appendage.

SPRING MECHANICS

Parts of the merus exoskeleton of the mantis shrimp raptorial appendage (Fig. 3A) can act as a spring and contract longitudinally. The maximum force required to fully contract the merus as well as the spring constant was used as proxies for the mechanical performance of the amplifier. We used previously published data from mechanical tests of the spring (Zack et al. 2009). These data were reanalyzed, because of an error discovered in the manufacturer's software used to drive the materials testing machine. The programming error caused the force data to be filtered, but not displacement data, resulting in a temporal offset in the two datasets. Using a Matlab program (version 2009a, The Mathworks, Natick

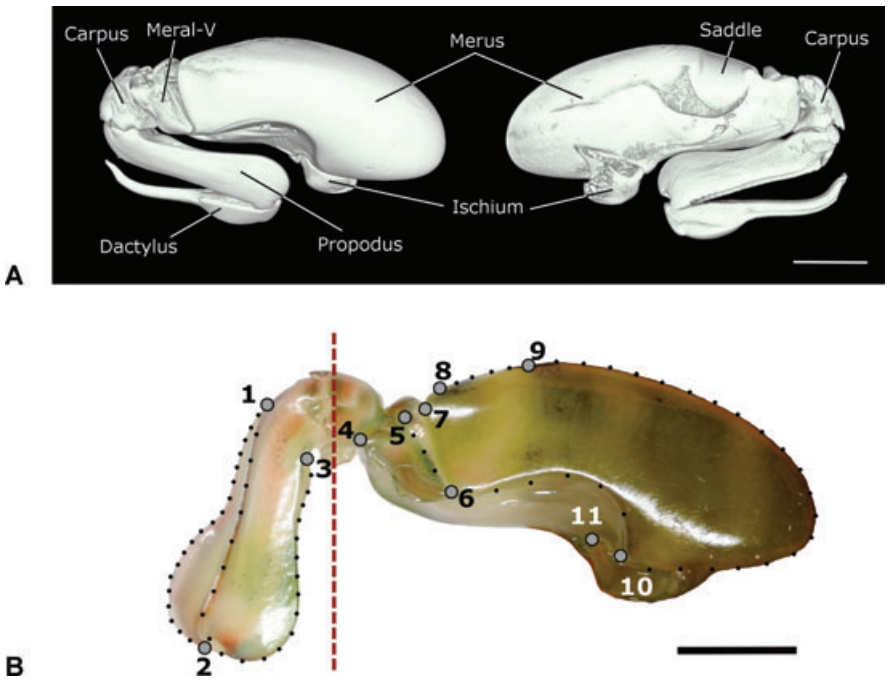

Figure 3. **The shape of the raptorial appendage was analyzed using geometric morphometric techniques. (A) A micro-CT scan of the lateral (left) and medial (right) sides of a *G. falcatus* appendage illustrate its five segments as well as the saddle and meral-V, two key components of the amplifier. (B) Landmarks (gray numbered circles) and semi-landmarks (small black dots) are shown on a photograph of the lateral view of a left raptorial appendage from *G. falcatus.* Note that the propodus/dactylus and merus were measured separately (dashed line), because it was not possible to standardize their relative positions. Scale bar 2 mm. Dorsal is toward the top of the page in all images.**

MA) written by the company to fix this error, we reanalyzed the data and calculated spring stiffness as the linear portion of the loading curve from 60% to 95% of the maximum load during loading and maximum force as the peak force generated during loading of the spring.

STRIKE FORCE

Peak strike force was measured for each individual and used as a proxy for strike performance (detailed methods are described in: Patek and Caldwell 2005). We used a one-axis force sensor to measure peak force (force range 3 kN, Model 9130B, Kistler Instruments, Winterthur, Switzerland). The stainless steel force sensor had an 8-mm diameter load surface and a stiffness of 1.0 $kN\mu m^{-1}$. Data were collected at 500,000 samples s^{-1} using a data-acquisition board (NIDAQ 6251, National Instruments, Austin, TX). Peak forces were analyzed using custom-designed computer analysis tools (R Development Core Team 2009). Each animal struck the force sensor at least 10 times; the peak force value of the strongest strike was used in subsequent analyses.

GEOMETRIC MORPHOMETRICS

The morphology of the raptorial appendages was characterized in two dimensions using geometric morphometric methods. Geometric morphometric methods yield detailed information about variation in the shape of objects while retaining a visual representation of them throughout the analysis (Mitteræcker and Gunz 2009).

Landmarks and semi-landmarks, which are coordinates of points upon which geometric morphometric methods are based (Bookstein 1991), were recorded from high-resolution digital images of left and right raptorial appendages using equipment designed to minimize distortion while maximizing definition and depth of field (12 megapixel, digital SLR camera, Nikon D300; AF Micro-NIKKOR 60 mm f/2.8D or 105 mm f/2.8D macro lenses, Nikon Inc., Melville, NY; and EM-140 DG macro-flash, Sigma Corp., Ronkonkoma, NY). Appendages were positioned in front of the camera using a custom-built device to maintain a consistent orientation across specimens and provide a linear scale. The lateral side of each appendage was photographed, first focusing on the merus and then focusing on the dactylus and propodus, with the dactylus folded against the propodus (Fig. 3B). Each specimen was photographed three times to evaluate measurement error from the coordinates of digitized landmarks and semi-landmarks. Photographs of the left appendages were mirrored to look like a right appendage prior to digitizing to facilitate symmetry analysis (Klingenberg and McIntyre 1998; Klingenberg et al. 2002). Landmarks and semi-landmarks were digitized using the software TpsDig2 (Rohlf 2005a).

Landmarks and semi-landmarks were superimposed (configurations scaled, rotated and translated) across specimens using the generalized least squares Procrustes method (Rohlf and Slice 1990). During superimposition, semi-landmarks were aligned using the minimal bending energy method (Bookstein 1997; Mitteröcker and Gunz 2009). Centroid size, which is the scaling factor during the superimposition process (Bookstein 1991; Dryden and Mardia 1998), was subsequently used as indicator of size for each specimen. The term "shape" used henceforth is defined as a geometric representation of an object (landmark configuration) remaining after removing information on its size and other measurement-associated error (rotation, translation).

Propodus/dactylus shape was quantified using three landmarks (from 1 to 3) and 42 semi-landmarks (Fig. 3B). Landmark 1 represents the visible distal tip of the dactylus (the actual tip was hidden inside a groove in the propodus); landmark 2 represents the proximal edge of the dactylus. Finally, landmark 3 represents the resting point for the carpus when the propodus is folded on the carpus (Fig. 3). Nineteen of the 42 semi-landmarks were placed between landmarks 1 and 2 to represent the ventral edge of the dactylus (opposite side to the edge in contact with the propodus). Nine semi-landmarks describe the dorsal edge of the propodus (edge in contact with the dactylus). The final 14 semi-landmarks were placed between landmarks 2 and 3 to represent the ventral edge of the propodus (opposite side to the edge in contact with the dactylus).

Merus shape was quantified using eight landmarks (from 4 to 11) and 32 semi-landmarks (Fig. 3B). Landmarks 4–6 describe the meral-V such that it would rotate around landmark 6. The meral-V is a triangular piece of the distal merus that is rotated proximally when the appendage is loaded (Fig. 1 and 3A). Landmarks 5–7 describe the opening between the meral-V and the rest of the merus. Landmarks 8 and 9 represent the relative position of the saddle on the merus; the saddle is a modification of the merus exoskeleton and compresses during merus contraction (Patek et al. 2007; Zack et al. 2009). Landmark 10 represents the ventral joint articulation linking the merus and the ischium. Finally, landmark 11 represents the point on the ventral merus that matches the tip of the ischium distal extension (Fig. 3). Three semi-landmarks were placed between landmarks 5 and 6 to represent the proximal edge of the meral-V and four semi-landmarks were placed between landmarks 8 and 9 on the dorsal edge of the merus, which represents the shape of the lateral edge of the saddle. Twenty semi-landmarks were placed between landmarks 9 and 10 to represent the proximal edge of the merus. Five semi-landmarks were placed between landmarks 10 and 6 to describe the lateral ventral edge of the merus. We did not measure the shape of the latch, because it was internal and exceedingly difficult to access in the context of these measurements.

Shape variation of the propodus/dactylus and the merus was first analyzed using a principal component analysis (PCA). This analysis is used to reduce the dimensionality of multivariate data by transforming a set of many correlated variables into a smaller number of uncorrelated variables called principal components. PCA was performed on shape data (partial warp scores, see Mitteröcker and Gunz [2009] review for details on partial warp scores computations) and allowed to condense shape information into as few principal components as possible to describe overall shape variation without a priori assumptions on the influence of size, sex, or appendage side (TpsRelw, Rohlf 2005b).

Symmetry

Bilateral symmetry in appendage shape and size (centroid size) was assessed separately for each sex and each part of the appendage (propodus/dactylus and merus) using a two-way analysis of variance (ANOVA) for size and a Procrustes ANOVA for shape (Klingenberg and McIntyre 1998; Klingenberg et al. 2002). Individual identity and appendage side (left or right) were the factors for these analyses. The random shape variation between left and right sides is called fluctuating asymmetry and is represented by the interaction term in the Procrustes ANOVA. This variable is important for later analysis (see developmental analysis below), but is generally of small amplitude. It is important to verify that measurement error (due to digitizing and photographic techniques) is not greater than the actual shape variation due to fluctuating asymmetry. For this, we ensured that the mean square values of the Procrustes ANOVA for the fluctuating asymmetry (interaction term) were higher than the mean square values of the error term (Klingenberg and McIntyre 1998; Klingenberg et al. 2002). Given that fluctuating asymmetry was detected in these tests, the next step was to calculate the actual values for the symmetric and asymmetric (fluctuating asymmetry) components of the appendages. This was done by calculating the mean shape coordinates for each specimen and using these as the symmetric component. We then calculated the residual variation (minus the error across replicates) from the average coordinates to yield the asymmetric component, which is the fluctuating asymmetry in this case. Significance levels were evaluated using 3000 bootstraps. The software Sage was used for calculations (Marquez 2008b).

Scaling

We tested the relationship between appendage size and body size for both sexes. Average left and right centroid size for the merus and the propodus/dactylus was used to represent appendage size, because the appendages were symmetric (see Results). Model II Reduced Major Axis regressions were applied and values were ln-transformed prior to analysis. We also tested whether size varied between sexes using an analysis of covariance (ANCOVA) with body length as the covariate and sex as the factor.

The symmetric component of appendage shape was then investigated in relation to appendage size (centroid size) using multivariate regression. Separate analyses were performed for the propodus/dactylus and the merus for both males and females. Significance level was estimated using 3000 bootstraps. The fluctuating asymmetric component of the shape variability was used to check whether random morphological variation was dependent on size.

Procrustes distance was the metric used to represent individuals' shape in graphs. This variable is a measure of the distance between two shapes in a "shape space" in which each individual has a unique location. For graphical representation, Procrustes distance is convenient, because shape of one individual (relative to a reference shape) is described with only one value.

The software regress6 (Sheets 2001) and R (R Development Core Team 2009) were used, respectively, for the multivariate and univariate regressions.

Sexual dimorphism

Sexual dimorphism in appendage shape was investigated by comparing the shape of the propodus/dactylus and merus (for the symmetric component only) between males and females. Shape difference between sexes was tested using a permuted multivariate analysis of covariance (per-MANCOVA, 1000 permutations) on shape variables (partial Procrustes distances, see Zelditch et al. [2004] for details) with sex as a factor and centroid size as the covariate. Centroid size was included as a covariate to correct for the effect of size on shape variation (see results). Per-MANCOVA was used instead of conventional MANCOVA, because the sample size was too small relative to the number of landmarks/semi-landmarks used in this study (Zelditch et al. 2004). The program Manovaboard 6.4 (Sheets 2006) was used for this analysis. This program uses a permutation test to determine significance (based on the sum of squared partial Procrustes distances—shape variables—between and within groups) rather than conventional MANCOVA procedure (i.e., using an F-test of a variance ratio).

Merus morphology and spring mechanics

Amplifier mechanics were expressed in terms of maximum force and stiffness. To analyze how spring mechanics correlate with scaling of merus shape variation, we used multivariate regressions. The shape variable of each particular appendage, rather than the symmetric component, was used for the analysis because the side of the appendage mechanically tested was known. Significance level was estimated using 3000 bootstraps. Spring force and stiffness were also regressed onto merus size (centroid size) using a linear regression. Sexes were not separated for this analysis because geometric morphometric methods require a large sample size and only 17 specimens were available, including six males and 11 females.

Propodus/dactylus morphology and strike force

We examined how shape variation correlates with impact force over a range of body sizes. Maximum strike force was investigated in relation to propodus/dactylus shape (symmetric component) and size (centroid size). The relationship between shape and force (separately in males and females) was analyzed using multivariate regression. To account for size differences, strike force was compared between sexes using an ANCOVA.

MODULARITY

We tested the hypothesis that the appendage is divided into three developmental modules that are the engine, the amplifier, and the tool (Fig. 1). Shape variation was used as a proxy to infer whether development was modular across the amplifier, engine, and tool. If the developmental pathways are such that these three units belong to different modules, one would expect that shape variation would be coherent within each unit but not between them, which is indicative of developmental integration within modules (Klingenberg and Zaklan 2000; Klingenberg et al. 2001, 2003; Klingenberg 2008). Conversely, congruent shape variation of all units of the appendage would indicate a developmental integration of the entire structure and refute the hypothesis of modular organization. In other words, if the shape variation between two units is always similar among appendages, then the structure would be considered as integrated; otherwise, each unit would belong to different modules.

Developmental modularity should not only be evident through variation across individuals, but should also be reflected by fluctuating asymmetry—shape variation between body sides (Klingenberg and Zaklan 2000). Because the left and the right sides of an individual share the same genome and nearly the same environment, fluctuating asymmetry results primarily from small random perturbations of developmental processes (Palmer and Strobeck 1986; Palmer 1996; Klingenberg and Zaklan 2000; Klingenberg et al. 2001, 2003, 2008; Hallgrímsson et al. 2002). Therefore, fluctuating asymmetry provides an intrinsic experimental "control" for genetic and environmental effects and indicates purely developmental processes. Correlated left and right asymmetries in two different regions of the appendage (that we will call partitions) thus indicate that the same perturbation has been transmitted to both partitions (Klingenberg and Zaklan 2000). Therefore, these two partitions are integrated and belong to a shared developmental pathway. The same conclusion could not be drawn regarding variation among individuals (measured with the symmetric component). This is because, contrary to fluctuating asymmetry, variation among individuals can be influenced by different genotypes or environments (Klingenberg 2008) and could not be ascribed solely to developmental processes.

Thus, if results from the fluctuating asymmetric component and the symmetric component show congruent shape variation, then the observed developmental pattern should be driven only by direct developmental interactions (Klingenberg et al. 2001; Klingenberg 2008). In other words, each module identified in the study would represent a developmental pathway resulting in an integrated region of the appendage. Conversely, incongruence between the results from the fluctuating asymmetric component and the symmetric component would indicate a parallel developmental pathway in which, for example, the development of two modules could covary due to synchronized responses of both pathways to a common environmental pressure (Klingenberg 2008). If the two modules covary for this reason, symmetric component analysis would only show a single module while the fluctuating asymmetric component analysis, which excludes environmental pressures from the shape variation, would lead to two distinct modules instead of one.

The first step in the modularity analysis is to divide the appendage into partitions. A partition is defined as a small region of the appendage represented by a subset of the total landmark configuration. Partitions can be selected randomly (Klingenberg 2009) or represent regions of particular morphological significance (Zelditch et al. 2009), such as an appendage segment or particular morphological feature. These partitions are thus the morphological units used to measure appendage regional shape variability and to detect modules that can be formed by single or multiple partitions. Appendage partitioning was performed after the merus and propodus/dactylus shapes were standardized relative to their respective averaged centroid size (separately for males and females). This step was necessary because ontogeny causes shape variation of different partitions to correlate with each other due to allometry (Zelditch et al. 2004). After standardization, shape data from both sexes were combined for the rest of the analysis.

The appendage was divided into five partitions (Fig. 4). The first partition ("dactylus") represents the dactylus and the second partition the propodus ("propodus"). The third partition ("distal merus") represents the distal part of the merus that acts as a spring and can be deformed during contraction (Fig. 4A, there are no muscle attachments in this region). The fourth partition ("proximal merus") represents the region of the merus where extensor muscles attach to the exoskeleton (Fig. 4A) and can consequently be used as a proxy to represent extensor muscle size. The fifth partition ("ventral merus") represents the ventral part of the merus where the flexor muscle attaches to the exoskeleton—this region possesses a curvature matching the propodus shape, which fits against the merus when the propodus is folded. Each of these partitions was individually superimposed and the fluctuating asymmetric component and the symmetric component were extracted from them.

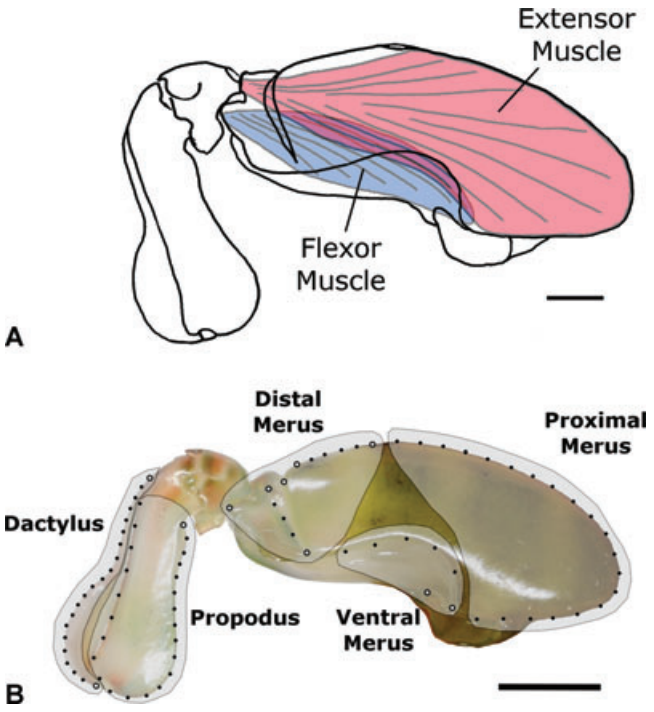

Figure 4. We used muscle attachment sites and segment anatomy to select appropriate regions to partition the appendage and test hypotheses on modularity. (A) The lateral extensor muscle occupies most of the space in the merus and is not attached to the exoskeleton in the ventral region of the merus. The flexor muscle is much smaller and attaches only in the ventral region of the merus. (B) To statistically analyze modularity between and among the regions of the raptorial appendage, six partitions (gray overlay on photograph) were chosen. The photograph shows the lateral side of a left appendage, dorsal toward the top of the page, distal to left. Scale bars: 2 mm.

Partition correlation

To test whether the shape variability of the appendage among specimens was congruent or organized into modules, we tested whether the magnitude of the shape variation of one partition among individuals matched the variation of other partitions (Mantel correlation test, Coriandis, Marquez 2008a). Partitions with correlated shape variation (congruent variability) would, therefore, belong to the same module and, conversely, partitions with shape variation that do not correlate would belong to different modules (Klingenberg 2008).

Correlations among the five partitions for each component (symmetric and fluctuating asymmetric) were calculated and stored in a correlation matrix using the software Coriandis (Marquez 2008a). To distinguish between a parallel developmental pathway and a direct developmental interactions pathway (see above and Klingenberg 2008), we tested whether the correlation matrix from the fluctuating asymmetric component was correlated with the correlation matrix from the symmetric component

(Mantel correlation test, vegan package of the software R, R Development Core Team 2009).

Hypothesis testing

We hypothesized that three developmental modules, representing the engine, amplifier, and tool, would occur in the raptorial appendage. Partitions 1 and 2 would belong to the tool module, partition 3 would represent the amplifier module, and partitions 4 and 5 would indicate the engine module (Figs. 1–4). To test this a priori hypothesis, we used two methods, the "target matrix method" and "graphical modeling."

For the target matrix method, we constructed a target theoretical correlation matrix among partitions with a correlation of one between every partition within each hypothetical module and a correlation of zero between partitions pertaining to different hypothetical modules (Cheverud et al. 1991). The correlation between the target correlation matrix and the data correlation matrix (fluctuating asymmetric component or symmetric component) was tested with a Mantel correlation test (R Development Core Team 2009).

For the second method, we used graphical modeling, which depicts the relationships among variables ("vertices") by drawing a line ("edge") to connect correlated variables (in this case, partitions) after taking their relationships to all other variables into account (Edwards 2000; Magwene 2001; Young and Hallgrimsson 2005; Allen 2008; Zelditch et al. 2009). We used graphical modeling to assess correlation networks among partitions (for the symmetric component and fluctuating asymmetric component of each partition) and evaluated the degree of correlation among them. We performed these analyses using a partial correlation matrix in which the matrix elements represented the pairwise correlation between pairs of partitions conditioned on their relationships with the other partitions. The partial correlation matrix can be calculated by inverting the correlation matrix from the fluctuating asymmetric component and the symmetric component and rescaling the new matrix such that the diagonals are all 1.0 (Magwene 2001).

To determine which edges should be included in the graphical model, we used a stepwise model selection procedure starting either from the fully saturated model (including every possible edge between variables) or the model that contains no edges at all. To test the significance of the correlation between two variables and determine whether an edge should be removed or not, we used an F-test because of the small sample size. Searches for the best model (most parsimonious and that best fits the data) were done headlong (edges inspected randomly rather than sequentially) and bidirectionally, proceeding first in one direction (i.e., deleting edges from a fully saturated model) and then in the other direction until the best model was found.

To assess the overall fit of the graphical model, we used the model deviance, which is a likelihood ratio of the specified model against the null hypothesis of the fully saturated model, with degrees of freedom equal to the number of excluded edges (Edwards 2000). The fully saturated model explains all the variance of the data (but is the least parsimonious, because it includes all possible edges). Thus, the best model should not be significantly different from the saturated model while possessing the fewest number of edges. The significance of a deviance difference (e.g., between a fully saturated model and best fitting model) can be tested using a χ^2 distribution (Edwards 2000). Finally, the edge strength, $\mathrm{Inf}(X_\mathrm{i} \perp X_\mathrm{j} \mid X_\mathrm{K})$, is a measure of the information in the element X_i about X_j and vice versa, conditional on the rest of the variables X_K. In other words, it indicates how strongly the two partitions are connected, conditional on the rest of the variables and can be calculated as:

$$Inf(X_i \perp X_j \mid \mathrm{X_K}) = -0.5 \cdot \ln\left(1 - \rho^2_{ij\cdot\{K\}}\right),$$

where $\rho_{ij\cdot\{K\}}$ is the partial correlation between the partition i and j (Magwene 2001). High edge strength is an indicator of strong co-predictability among traits relative to all the others and low edge strength indicates low co-predictability.

Results

GEOMETRIC MORPHOMETRICS

PCA provided a descriptive analysis of the variation in appendage shape without assumptions about the effect of sex, size, or appendage size. The first three axes of the PCA explained 90.11% of the total shape variation for the propodus/dactylus (tool) and 62.49% of the total shape variation for the merus (amplifier and engine).

For the propodus/dactylus, the first axis (77.19% of the total shape variability) described a narrowing of the propodus along the dorsoventral plane and a reduction of the dactyl bulb (Fig. 5A)—the dactyl bulb is the bulbous, rounded part of the proximal region of the dactylus that is used as a hammer (Fig. 3). The second and third axes explained 8.60% and 4.32% of the shape variability, respectively. The second axis represented a ventral elongation of the dactyl bulb along the distal propodus margin (Fig. 5A) whereas the third axis described a narrowing of the dactylus along the dorsoventral plane. It is interesting that within these results, males had greater shape variation than females; this variation was described by the first axis of the PCA (Fig. 5A).

For the merus, the first axis of the PCA (34.26% of the total shape variability) described an increase of the ventral curvature when the overall height of the merus decreases (Fig. 5B). The second axis (16.69% of shape variation) described a decrease of

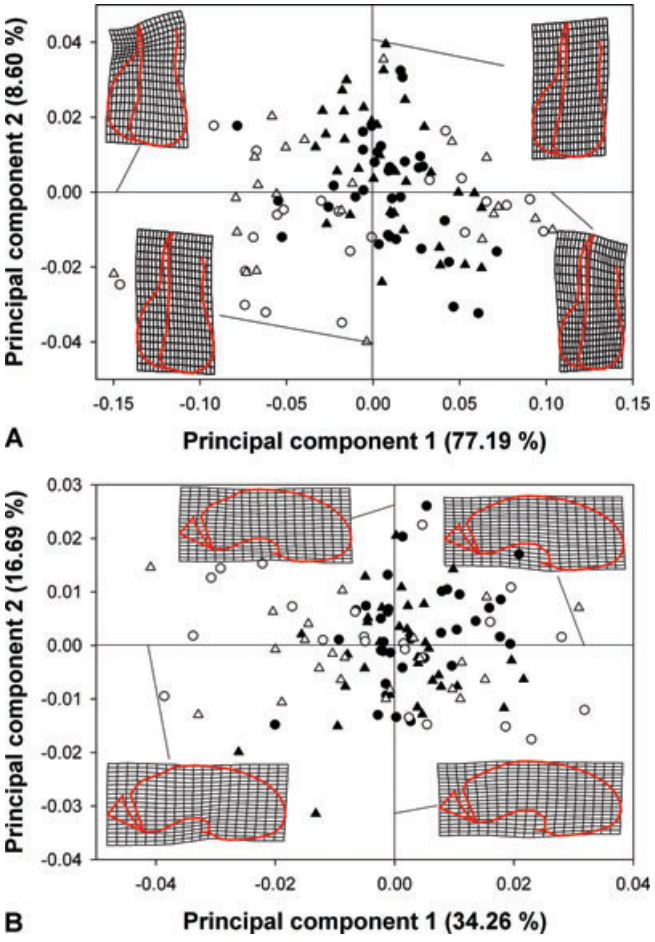

Figure 5. Principal component analyses identified the primary axes of variation in shape. (A) For the propodus/dactyl, the first and second principal component described together 86% of the variation. (B) For the merus, the first and second principal component explained together 51% of the variation. The deformation grid (thin-plate spline) illustrations of the appendage segments represent the extreme shape variation along the different principal components. The percentage explained for each axis is indicated in parentheses on the graphs. The symbols are as follows: left appendages (circles), right appendages (triangles), males (white-filled symbols), females (black-filled symbols).

the ventral curvature and the third axis (11.53% of the shape variation) described an increase of the proximal distance between the dorsal and ventral edges of the merus (Fig. 5B). Similar to the propodus/dactylus results, males exhibited a greater range of shape variation than females, described by the first principal component (Fig. 5B).

Symmetry

Results of the Procrustes ANOVA showed no significant differences between left and right sides for propodus/dactylus and merus shape for both males and females, with the exception of one borderline significant result in female merus shape that explains only 2% of the shape variation (Table 1). Similarly, ANOVAs of centroid size did not show any significant difference in symmetry across the propodus/dactylus, merus and across the sexes (Table 1). Overall, these results indicate that this species is symmetric in shape and size for both the propodus/dactylus and the merus.

We found significant differences in shape and size among individuals for propodus/dactylus and merus as well as sex, indicating individual variability (Table 1).

The mean square values of fluctuating asymmetry in the Procrustes ANOVAs were always greater than the mean square values from the error terms (which represented at most 16% of the fluctuating asymmetry). Fluctuating asymmetry was always significant for the merus and propodus/dactylus of both sexes (Table 1).

Scaling

Propodus/dactylus size (centroid size) was positively correlated with body size for males (slope = 1.02, 95% CI = 0.93–1.12; $r^2 = 0.96$) and females (slope = 0.99, 95% CI = 0.93–1.06; $r^2 = 0.97$). There was also a significant interaction between sex and propodus/dactylus size ($F_{1,52} = 9.90$, $P = 0.003$, Fig. 6A) meaning that the difference in appendage size between sexes was dependent on animal size. However, these differences were very small. Merus size (centroid size) was also positively correlated with body size for males (slope = 1.12, 95% CI = 1.04–1.20; $r^2 = 0.98$) and females (slope = 1.02, 95% CI = 0.96–1.09; $r^2 = 0.97$) and there was a significant effect of the interaction between sex and merus size ($F_{1,52} = 21.1$, $P < 0.001$, Fig. 6B) meaning that there was sexual dimorphism with large males having a greater appendage size (allometry) than large females.

Propodus/dactylus shape changed significantly with appendage size for males, but not for females (Table 2). The multivariate regression showed that 67% of the total male propodus/dactylus shape variation was explained by size (Table 2). From small to large males, shape changes were similar to the ones described by the first axis of the PCA—an increase of the dactyl bulb curvature for the proximal dactylus and distal propodus (Fig. 7A). This shape variation was clear in males, but nearly absent in females (Fig. 7A). Merus shape changed significantly depending on appendage size for males and females (Table 2). The multivariate regression showed that size explained 42% and 13% of the total merus shape variability of males and females (Table 2). From small to large animals, merus shape variation was comparable to the variability explained by the first axis of the PCA, which was mainly a decrease of the curvature of the ventral part of the merus (Fig. 7B).

No significant relationship was found between the fluctuating asymmetric component and appendage size for males and females (Table 2).

Table 1. The presence of morphological variation in bilateral symmetry (Side) and among specimens (Individuals) as well as the detection of fluctuating asymmetry (Interaction) were analyzed with a Procrustes ANOVA for the shape variable and with a conventional ANOVA for the size variables. Analyses were performed independently for males and females and for the propodus/dactylus and merus. ANOVA's *F*-values and *P*-values calculated using 3000 Bootstraps are reported. Bold *P*-values indicate significant results.

Variable \ factors	Individuals (*F*-value)	*P*	Side (*F*-value)	*P*	Interaction (fluctuating asymmetry) (*F*-value)	*P*
Propodus/dactylus male (shape)	18.26	**<0.001**	1.50	0.216	11.86	**<0.001**
Propodus/dactylus male (size)	302.66	**<0.001**	1.09	0.325	10.13	**<0.001**
Propodus/dactylus female (shape)	3.72	**<0.001**	2.33	0.093	18.32	**<0.001**
Propodus/dactylus female (size)	221.78	**<0.001**	1.36	0.260	13.94	**<0.001**
Merus male (shape)	4.62	**<0.001**	1.03	0.389	7.38	**<0.001**
Merus male (size)	370.57	**<0.001**	0.00	0.922	3.40	**<0.001**
Merus female (shape)	2.83	**<0.001**	2.93	**0.024**	6.13	**<0.001**
Merus female (size)	1684.70	**<0.001**	0.00	0.998	13.10	**<0.001**

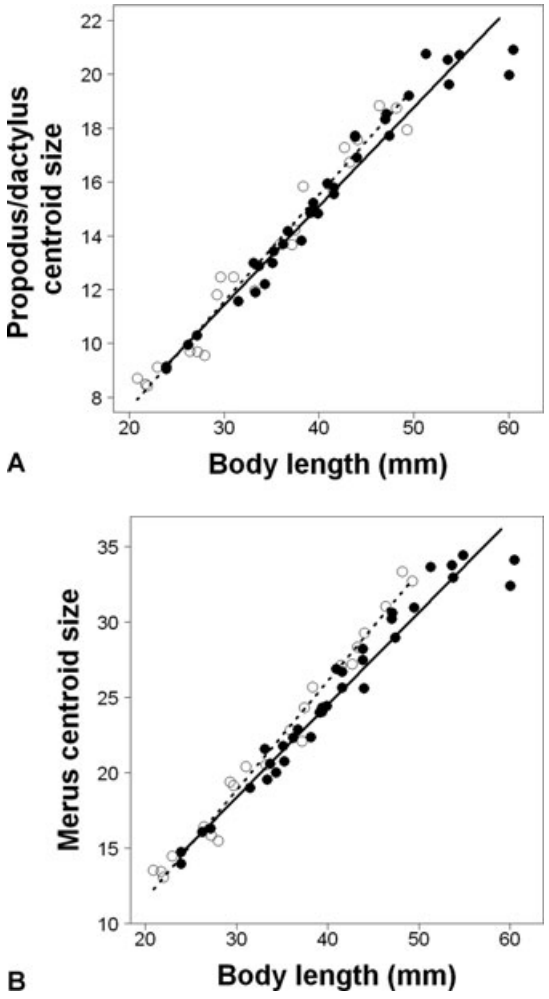

Figure 6. Body length (mm) was positively correlated with both propodus/dactylus centroid size (A) and merus centroid size (B). Similar trends were found for males (white-filled circles; dashed regression lines) and females (black-filled circles; solid regression lines).

Sexual dimorphism

Results from the Per-MANOVA showed that there was a significant difference in merus and propodus/dactylus shape between males and females depending on appendage size (merus: $P < 0.002$, propodus/dactylus: $P < 0.002$). Large males appeared to have a bulkier propodus/dactylus than females (Fig. 7A). Merus differences were subtle and indicated that males had a dorsoventrally wider merus that was more ventrally curved than females (Fig. 7B).

Table 2. Multivariate regressions were used to test whether appendage shape variation was related to appendage size. Symmetric component (Sym) and the fluctuating asymmetric component (FA) of the appendage shape were tested for males and females. Goodall *F* test was specifically developed for morphometric analyses and is equivalent to *F*-values for univariate analysis. Variance in the data explained by the regression (percentage explained) is shown and *P*-values were calculated from 3000 bootstraps. Bold *P*-values indicate significant results.

Variables	Goodall *F*	Percentage explained	*P*
Male propodus/dactylus (Sym)	41.25	67.35	**<0.001**
Female propodus/dactylus (Sym)	2.30	6.71	0.082
Male merus (Sym)	14.47	41.99	**<0.001**
Female merus (Sym)	4.86	13.18	**<0.001**
Male propodus/dactylus (FA)	0.47	2.27	0.652
Female propodus/dactylus (FA)	1.03	3.12	0.325
Male merus (FA)	1.27	5.96	0.257
Female merus (FA)	0.61	1.86	0.690

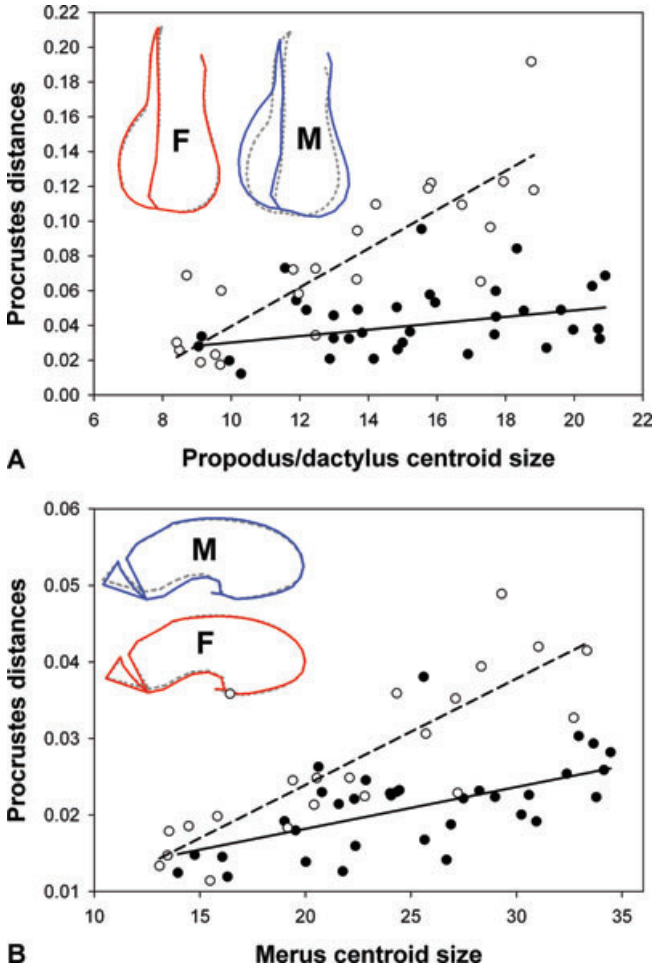

Figure 7. Procrustes distance was positively correlated with both propodus/dactylus centroid size only for males (A) and merus centroid size for both sexes (B). Procrustes distance represents the shape distance between an individual's shape and the smallest specimen's shape of the comparison group. The associated extreme landmark configuration is the illustration shown above the curve and represents the overlaid changes from small individuals (dotted) to large animals (solid). Males (M illustration, white-filled dots; dashed regression lines) yielded greater allometric scaling than females (*F* illustration, black-filled dots; solid regression lines).

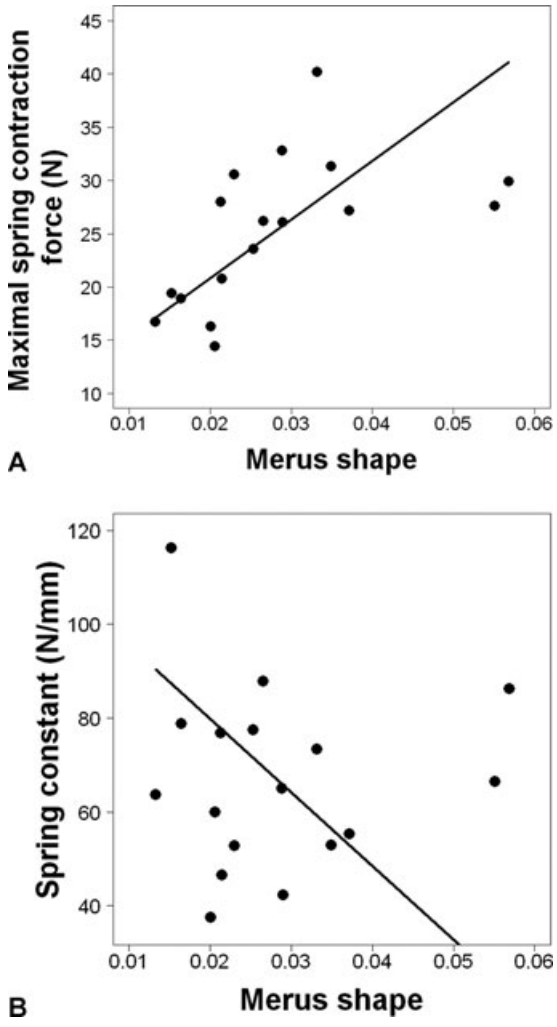

Figure 8. Maximal spring contraction force is nearly positively correlated with merus shape (A) whereas the spring constant is not correlated with merus shape (B). Merus shape is calculated as the Procrustes distance of each individual compared to the smallest individual of the comparison group.

Merus morphology and spring mechanics

Maximum spring force was positively correlated with merus centroid size (slope = 1.01, $r^2 = 0.61$, $F_{1,15} = 23.1$, $P < 0.001$), but spring stiffness was not ($F_{1,15} = 2.61$, $P = 0.127$).

Multivariate regressions showed that spring force and spring stiffness were not correlated with merus shape (force: Goodall's $F_{44,660} = 1.790$, $P = 0.125$; stiffness: Goodall's $F_{44,264} = 0.293$, $P = 0.946$). A closer examination of the data indicates that, although not significantly correlated, spring force followed a positive association with merus shape, indicating that the negative statistical result could be a consequence of poor sample size (Fig. 8).

Propodus/dactylus morphology and strike force

Strike force was positively correlated with the propodus/dactylus centroid size (slope = 6.92, $r^2 = 0.57$, $F_{1,41} = 60.51$, $P < 0.001$), but there was no difference between males and females ($F_{1,41} = 0.88$, $P = 0.354$, Fig. 9A).

Strike force was investigated separately for males and females, because of the propodus/dactylus shape differences between sexes. Multivariate regression showed that propodus/dactylus shape of males was related to strike force (Goodall's $F_{44,572} = 10.55$, $P = 0.002$) in the same way that shape variation was related to size. However, the shape of female propodus/dactylus was not related to strike force (Goodall's $F_{44,1232} = 1.76$, $P = 0.152$), which is consistent with the fact that female propodus/dactylus shape does not vary much (Fig. 9).

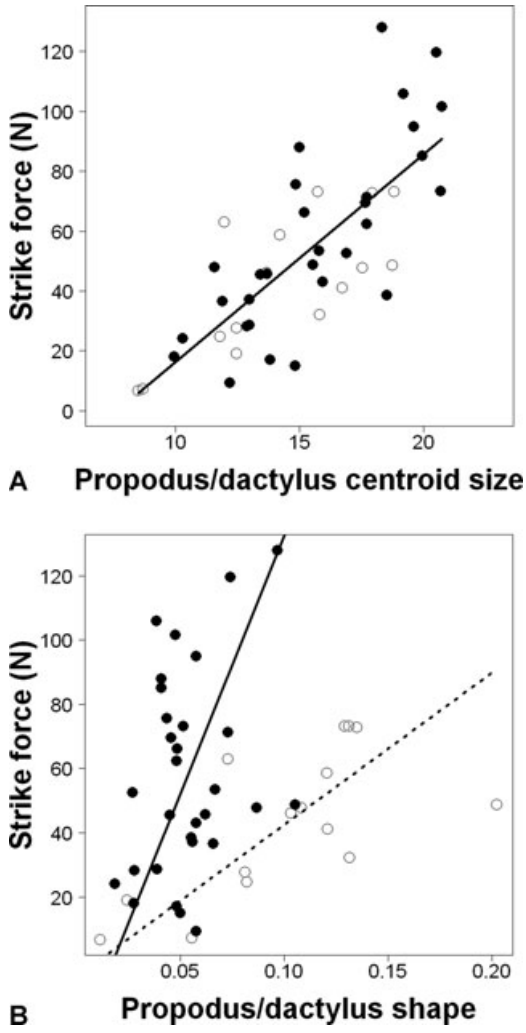

Figure 9. Maximum strike force is positively correlated with propodus/dactylus centroid size (A), and with male propodus/dactylus shape (B). Propodus shape is calculated as the Procrustes distance of each individual compared to the smallest in that group. Females (black-filled circles, black line) and males (white-filled circles, dotted line) are combined in analyses using centroid size (A) but separated in analyses using shape (B).

MODULARITY

Partition correlation

The correlation matrix of the symmetric component was correlated with the correlation matrix of the fluctuating asymmetric component (Mantel $r = 0.961$, $P = 0.017$, 3000 permutations), indicating a direct developmental pathway rather than a parallel developmental pathway.

Hypothesis testing

Using the target matrix method, we tested whether the appendage was organized into three developmental modules following the pattern: engine, amplifier, and tool. There were no significant correlations between the theoretical correlation matrix and the symmetric component correlation matrix (Mantel $r = 0.947$, $P = 0.067$, 3000 permutations). There were also no significant correlations between the theoretical correlation matrix and the fluctuating asymmetric component correlation matrix (Mantel $r = 0.881$, $P = 0.064$, 3000 permutations). Although nonsignificant, these results show large correlation coefficients ($r > 0.8$) that indicate that the nonsignificance is most likely a result of a small sample size.

Graphical modeling yielded the same results both for the fluctuating asymmetric and symmetric component (Fig. 10). Both of these graphs do not differ significantly from the fully saturated model (symmetric component: $\chi^2 = 8.76$, df $= 8$, $P = 0.363$; fluctuating asymmetric component: $\chi^2 = 9.57$, df $= 8$, $P = 0.295$). The most parsimonious models explain 90.72% of the total symmetric shape variation and 91.94% of the total fluctuating asymmetric shape variation. These graphs show that the shape variation of the dactylus and propodus match well and belong to the same module (edge strength for the symmetric component: 0.60; for fluctuating asymmetric component: 0.85). The spring part of the merus is linked neither to the propodus/dactylus nor to the rest of the merus and appears to be an independent module. The proximal and ventral parts of the merus appear to belong to the same module and share an edge-strength of 0.17 for the symmetric component and 0.13 for the fluctuating asymmetric component (Fig. 10).

Discussion

By examining a power amplification system in terms of an engine, amplifier, and tool, we were able to test how the shape and size of these units contributes to the system's function as a whole and also how these units vary relative to each other. We found that shape variation in each of these units could be explained by sex and body size, with different scaling factors depending on the unit. Strike force is positively correlated with appendage size and is not sexually dimorphic. Similarly, spring force is positively correlated with size, but spring stiffness is not. Each unit is developmentally modular, suggesting that changes in one unit could occur independently of others.

This iterative, quantitative approach of looking at each unit's size and shape in the context of the broader function of the system provides a new window into the evolutionary liability and biomechanical dynamics of power amplification systems. We will examine in greater depth each of these results below in parallel with current knowledge about the scaling of power-amplified systems. Although many power-amplified systems have been described, such as tongue protrusion in amphibians and reptiles or flight in insects, scaling of such systems have, to our knowledge, only been studied in vertebrate jumping mechanisms and a few jumping and striking arthropods (Alexander et al. 1981; Biewener 1989;

Katz and Gosline 1992; Pollock and Shadwick 1994a; Zack et al. 2009). Following the examination of the results, we will discuss the broader implications of these findings in relation to potential evolutionary pathways that power-amplified systems could follow.

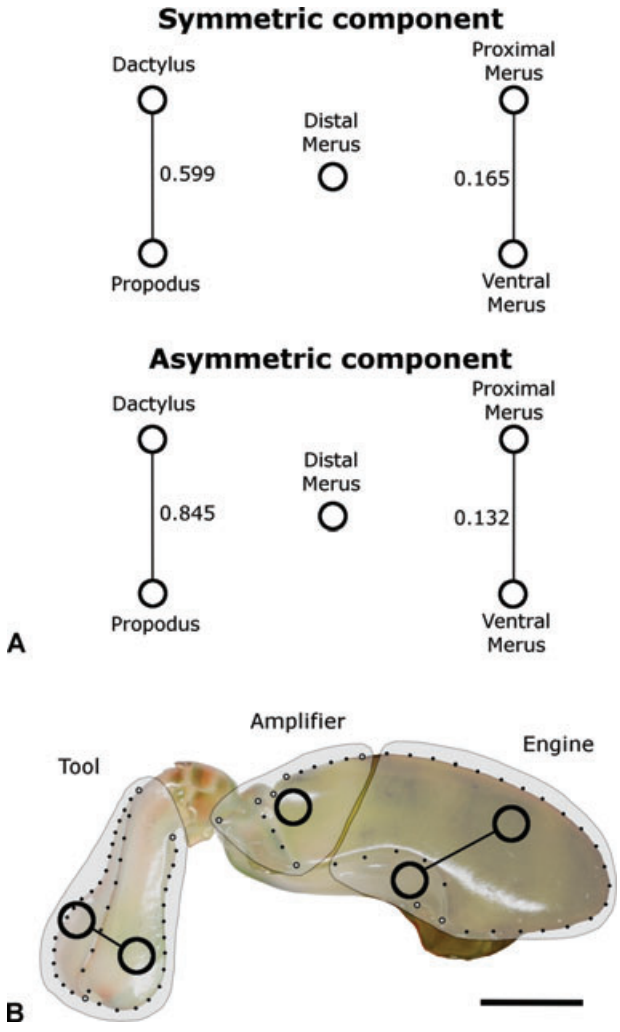

Figure 10. Graphical models depict the strength of associations among the partitioned appendage structures and indicate whether developmental modularity is present in this system. Links (edges) connect the circles (representing partitions) that are significantly correlated. Higher correlation values (the number to the side of the model "edge"), indicate a greater association between the partitions. (A) Graphical models show similar results for the symmetric components and the asymmetric components where variation of the dactyl and propodus are more tightly correlated than the variation between the proximal and ventral merus. The distal merus shows no correlated change with the other partitions. These results indicate that the dactylus-propodus, distal merus, and ventral-proximal merus are different developmental modules. (B) The modules are represented in gray with the associated graphical modeling results overlaid on the photograph of the appendage. Scale bar: 2 mm.

SCALING

The engine, amplifier, and tool of *G. falcatus*' raptorial appendage exhibit different shapes depending on size and sex, and each unit scales differently from the other units. Beginning with the most fundamental level, sexual dimorphism, males have slightly larger appendages than females. This sexual dimorphism in overall size impacts both scaling and size-dependent shape variation between the two sexes as we will discuss below. Following from this, we can look at the scaling and shape variation of each unit, beginning with the engine.

Engine

The engine, represented by the proximal part of the merus, grows isometrically (Figs. 4A and 7B). This finding is based on the assumption that the extensor muscle occupies most of the space in this unit of the appendage, which we observed through dissections in this and other studies. The muscle physiology may vary within the constraints of the available space (Taylor 2001), but many studies on crab claws have shown that shape of the claw is a good proxy for muscle force (Blundon 1988; Lee 1993; Gabbanini et al. 1995; Levinton et al. 1995; Block and Rebach 1998; Schenk and Wainwright 2001; Taylor 2001; Mitchell et al. 2003; Claverie and Smith 2007). Although a more rigorous evaluation of muscle performance in relation to size would be needed, we can reasonably assume that muscle force increases proportionally to muscle shape and size, as seen in other crustaceans (Mitchell et al. 2003; Claverie and Smith 2007).

The scaling of the stomatopod engine, which appears not to change in shape relative to size, differs from the findings in jumping and running mammals. In mammals, the scaling of the "engine," which consists of ankle extensor muscles, has a mass that scales isometrically with body mass (Alexander et al. 1981; Pollock and Shadwick 1994a), but a shape that changes allometrically. The muscles become stronger (greater cross-sectional area), but shorter as the animal increases in size (Alexander and Bennet-Clark 1977; Alexander 1981; Alexander et al. 1981; Pollock and Shadwick 1994a). We were unable to find a published study investigating the scaling of the "engine" (muscle) in arthropod power-amplified structures.

Amplifier

The amplifier of *G. falcatus* scales allometrically; as the merus increases in size, the dorsoventral part of the distal merus region elongates to a greater extent than the rest of the merus. Given that males have a larger merus relative to females, their spring becomes relatively larger as animals increase in size, but also exhibits greater allometry in the shape of this unit. Furthermore, given that the amplifier is primarily composed of two calcified bands that act as tape springs (Patek et al. 2007; Zack et al. 2009), this elongation of the spring should result in a longer lever arm

for the extensor muscle to contract. In other words, when the tape spring increases in length, the muscle that pulls at the end of the spring has a greater leverage and the spring bending should be easier (assuming a constant stiffness).

Spring stiffness and maximal force show different scaling relationships relative to size and shape of the merus. Only spring stiffness and maximal force were chosen to represent spring mechanics, because they were found to be the most representative variable to characterize this system (Zack et al. 2009). Spring elongation and maximal spring force are positively associated, but not significantly correlated (Fig. 8A), possibly due to small sample sizes. Moreover, maximal spring force is positively correlated with merus centroid size whereas stiffness is not. As said above, the elongation of the spring in the amplifier with increasing size of the appendage should provide greater leverage for the extensor muscle. The spring should also increase in stiffness with increasing size, given that the arthropod exoskeleton generally increases in stiffness when animals grow larger (Borrell 2004; Katz and Gosline 1994). However, given that we did not find a positive correlation between spring stiffness and size, this result suggests that the material properties, material distribution, or simply the leverage on the spring is changing ontogenetically, perhaps to accommodate constraints on muscle force generation with increasing size (Taylor 2001; Zack et al. 2009).

In vertebrates, scaling of the "amplifier"—the ankle extensor tendon in their limbs—is typically morphologically isometric relative to body mass, whereas elastic energy storage is positively and allometrically related to body mass (Alexander et al. 1981; Peterson et al. 1984; Pollock and Shadwick 1994a, b). Thus, tendons of larger species operate under smaller safety factors (the ratio between load that causes failure and the maximum load experienced during daily use) (Alexander 1974; Biewener et al. 1981; Alexander et al. 1982; Dimery and Alexander 1985; Dimery et al. 1986; Biewener and Blickhan 1988; Ettema 1996; McGowan et al. 2008).

In arthropods, we found only two published studies about scaling in amplifiers. During the ontogeny of jumping locusts, the shape of tibia (amplifier) changes allometrically; the tibia are longer and more slender than expected by isometry, whereas stiffness scales isometrically relative to body mass (Katz and Gosline 1992, 1994). However, these studies may not have focused on the most relevant amplifier in locust legs; most elastic energy storage occurs in the semi-lunar process whereas the tibiae store only approximately 10% of the elastic energy (Bennet-Clark 1975; Katz and Gosline 1992; Gronenberg and Ehmer 1996). More recently, a study of the amplifier in the raptorial appendages of mantis shrimp revealed that elastic energy stored in the amplifier scales proportionally with appendage size whereas stiffness does not (Zack et al. 2009). Scaling differences in spring stiffness in mantis shrimp and locusts could be the result of different allometric shape changes or changes in exoskeletal material composition during ontogeny leading to different mechanical properties of the spring.

One interesting area for future study is the scaling and shape variation of latches in power-amplified systems. Scaling of latches relates closely to balancing mechanical advantage relative to the large, antagonistic spring-loading muscles of most power-amplified systems (Burrows 1969; Burrows and Hoyle 1972; Gronenberg 1995a, b). The other component of latch performance is the rate at which it releases stored elastic energy in the amplifier. To fully understand the integration of these systems, latch shape, scaling and mechanics warrant further study.

Tool

The tool (propodus/dactylus) is bulkier in stomatopod males; specifically, males show allometric changes in the propodus/dactylus shape, such that larger appendages have a bulkier distal (hammer) region of the propodus and dactyl. However, strike force is not sexually dimorphic; peak forces are explained only by appendage size and not sex. Given that the bulkier hammer is not associated with a greater force output of the system, it is possible that shape sexual dimorphism can be explained by different uses of the hammer in males versus females. For example, mammalian horns are bulkier in males of species that engage in "ramming" behavior (Schaffer 1968; Lundrigan 1996). Similarly, thicker skulls were found in ramming dinosaurs (Barghusen 1975; Snively and Cox 2008).

Sexual dimorphism is commonly observed in decapod crustaceans; however, its role in mantis shrimp behavior is not clear. Male crabs and lobsters typically have larger claws than females and exhibit a greater range of shape variation (Hartnoll 1974; Stein 1976; Claverie and Smith 2009, 2010). This pattern has generally been explained by the fact that males are frequently involved in intrasexual fighting and larger claws are stronger and confer an advantage (Barki et al. 1992; Sneddon et al. 1997, 2000; Claverie and Smith 2007). Furthermore, in the particular case of fiddler crabs, greater claw size has also been explained by promoting mate attraction (Crane 1975). Both sexes of stomatopods engage frequently in intraspecific interactions during which they display the merus, but not the tool (Caldwell 1975). However, when breeding pairs are formed in *Neogonodactylus bredini*, males assume the sole responsibility for the defense of the breeding cavity (Shuster and Caldwell 1989). Consequently, the absence of strike force dimorphism suggests that other parameters such as strike frequency rather than force would be more relevant to explain the observed sexual dimorphism. Future studies incorporating 3D scaling analyses of tool shape and fluid dynamic analyses are required to fully understand the functional implications of these findings.

Other scaling studies of power-amplified mechanisms have focused on the tools used in jumping or running. In jumping

and running vertebrates, the "tool" is the foot, which acts as a lever system. One side is articulated at the ankle and connected to the extensor tendon whereas the other side pushes against the ground. Generally, the mechanical advantage of the mammalian foot is thought to increase allometrically relative to body mass (Biewener 1989). One exception to this rule is found in kangaroos, which keep a constant mechanical advantage regardless of body mass (Biewener 1989; Bennett and Taylor 1995).

Thus, the performance of the engine, amplifier, and tool of vertebrate jumping systems are all positively correlated with body mass, which is consistent with the fact that jumping performance also scales with body mass. Simply put, large animals jump relatively further than small animals (Choi et al. 2000; Wilson et al. 2000; James et al. 2007).

In arthropods, the scaling of the power-amplified "tools" and their performance have been characterized in mantis shrimp (Patek and Caldwell 2005), trap-jaw ants (Gronenberg and Ehmer 1996; Patek et al. 2006; Spagna et al. 2008), and locusts (Katz and Gosline 1993). A study of a mantis shrimp, *O. scyllarus*, examined the scaling of tool size and force generation; the larger the hammer surface, the greater the peak force generated (Patek and Caldwell 2005). Within and across trap-jaw ants, a polyphyletic group of ants that use their mandibles to capture prey or jump (Gronenberg and Ehmer 1996; Patek et al. 2006), mandible size increases isometrically with body mass (Spagna et al. 2008). Jump performance was not measured in relation to scaling in trap-jaw ants, but mandible strike force was proportional to the size of the head (Spagna et al. 2008). In locusts, jump performance, in terms of take-off velocity, was independent of body size within adults and within juveniles (Katz and Gosline 1993).

MODULARITY

In mantis shrimp, both symmetric and fluctuating asymmetric components showed the same pattern in shape variability, which indicated the presence of three developmental modules. When both symmetric and asymmetric components show the same modular pattern, this indicates that a direct interaction pathway is driving the development of the structure (Klingenberg and Zaklan 2000; Klingenberg et al. 2001, 2003). Consequently, our results suggest that we correctly identified the developmental units of the appendage.

The graphical modeling approach suggests that each unit belongs to a different developmental module, but the target matrix approach yields less clear-cut results. The shape variation of the proximal and ventral regions of the merus (engine) and the propodus and dactylus (tool) is correlated, but the shape variation of these four partitions are not correlated with the shape variation of the distal region of the merus (amplifier). Based on the target matrix analyses, shape variation among these three different units is neither perfectly independent nor perfectly internally coherent, yet the graphical modeling approach yielded a strongly modular structure (Fig. 10). The different findings from these two methods reflect the fact that the target matrix method assumes an all-or-none dependence/independence relationship among partitions, whereas graphical modeling does not. Typically, modular structures are rarely perfectly isolated and a covariance between modules never equals zero (Klingenberg et al. 2003).

Small interactions between modules have been measured in many systems such as bumblebee wings, rodent mandibles, or fowl body morphology (Klingenberg et al. 2001; Magwene 2001; Klingenberg et al. 2003; Zelditch et al. 2009). For example, in mice mandibles, developmental modules that represent the distal section of the mandible covary slightly with the modules that represent the proximal region (Klingenberg et al. 2003). This is because the processes that generate intramodular association may overlap spatially (Marquez 2008c). In that context, explorative methods such as graphical modeling might be better suited than the simple but less-flexible approach of target matrices for studying modularity patterns (Magwene 2001; Zelditch et al. 2009). Furthermore, even if the target matrix approach did not show any significant similarities between the theoretical modular structure (engine, amplifier, and tool) and the observed shape variation, there was a relatively high correlation between these matrices (>0.85), which is consistent with graphical modeling results.

Overall, these results indicate that the functional units of the mantis shrimp's appendage—the engine, amplifier, and tool—each belong to a different developmental module. Although not previously studied in power-amplified systems, a match between developmental modules and functional modules has been found in many other systems. For example, in mice mandibles, the functional units that correspond to muscle attachments on one side and to the presence of teeth on the other side each belong to a different developmental module (Atchley et al. 1985; Cheverud et al. 1991; Mezey et al. 2000; Klingenberg et al. 2003).

The consequences of a modular organization are many. For example, each unit could be independently tuned to its particular function during ontogeny and evolution (Wagner 1996; West-Eberhard 2003), while maintaining a functioning power-amplified system. Because each module is independent, mutation occurring in the pathway of one module will not affect others. Conversely, selective pressures affecting only one module will only affect the portion of the genome regulating the pathway of this module. Consequently, modular organization of an organism increases evolvability and specialization by reducing pleiotropy (Wagner and Altenberg 1996; Waxman and Peck 1998; Schlosser 2002).

MODULARITY AND THE EVOLUTION OF POWER AMPLIFICATION

In the context of the evolution of the power-amplified system in *G. falcatus*, it is particularly interesting to note that

different modules could change differently depending on sex or size. For example, change in amplifier shape depending on appendage size is possible without changes to other units; this may indeed be necessary if the mechanical consequences of increasing exoskeletal size do not correspond directly to the increased force output of the muscle across the same size range. Such a difference in ontogenetic trajectories (isometry vs. allometry) among modules could have evolved according to different selective pressures acting on them (Wagner 1996; West-Eberhard 2003). For example, the difference in the scaling of tool shape between sexes could be a direct consequence of different striking behavior between males and females (Shuster and Caldwell 1989), while also constrained by some minimal functional requirement (i.e., tool too small/large might be mechanically inappropriate). More broadly, modular development of mantis shrimp raptorial appendages may have released the tool to be morphologically variable while still driven by the same power amplification system. The tremendous diversity of mantis shrimp tools, from hatchets and hammers to spears (Ahyong 2001), certainly lends credence to this idea.

More generally, a comparison of our results with the scaling of other power-amplified systems allows us to note general trends as well as highlight the differences specific to a particular usage of these systems. For example, power-amplified structures follow different ontogenetic trajectories (isometry vs. allometry) depending on the functional unit. In mammals, the engine and tool follow allometric morphological changes, whereas the amplifier follows an isometric change relative to size. In mantis shrimp, it is the engine and the tool of females that follow isometric changes whereas the amplifier and the tool of males changes allometrically with body size. These scaling differences among the engine, amplifier, and tool, irrespective of the usage of the power-amplifying structure or the taxonomic group, suggest that a modular organization could generally occur in power-amplified systems.

Scaling differences between mammalian jumping and mantis shrimp striking could be due to two main differences. First, vertebrates possess an endoskeleton, which means that the volume that a muscle can reach during development is not limited by an exoskeleton as it is in arthropods. Second, jumping performance is tightly bound to animal mass. By definition, jumping performance will be determined by the acceleration of the body mass, whereas striking performance need not be related to animal mass. In vertebrate power-amplified systems, the need to match muscle force with animal mass may have led to the evolution of greater muscle force (i.e., greater diameter) relative to animal size. Furthermore, the release of the muscle from the spatial constraint as the one imposed by the exoskeleton in arthropods, might have enhanced allometric growth of the engine in vertebrates. Conversely, in mantis shrimp, the engine might be spatially constrained by exoskeleton, but not bound to animal mass. As a result, selective pressure on this system might have acted only on the evolution of amplifier scaling properties during ontogeny to match engine force and maximize strike speed. Additional cross-species studies of scaling in power-amplified systems are likely to yield important insights into the evolution of ontogenetic pathways relative to the selective pressures exerted on the engine, amplifier, and tool.

CONCLUSIONS

The framework developed here, in which we divide a power-amplified structure into an engine, amplifier, and tool, provides a useful approach to studying the evolutionary history of fast movements in nature. Assuming that each functional unit belongs to different developmental modules, simple morphological or biomechanical variables could be attributed to each functional unit and could be compared across species using phylogenetic comparative methods (Felsenstein 1985). However, the limits of the present approach lie in the uncertainty of the spatial boundaries among functional units in some systems. For example, in very small jumping mammals, the muscle acts as an amplifier. In these species, tendons are not stretched (because they are too robust compared to muscle force and animal mass) and the recoil of stretched muscles is sufficient to act as an amplifier (Alexander and Bennet-Clark 1977; Biewener et al. 1981; Pollock and Shadwick 1994a; Ettema 1996). In this particular case, the amplifier and engine spatially overlap but could still be developmentally and functionally separated, because muscle elasticity is related to muscle length whereas contraction force is related to muscle cross-sectional area (Alexander and Bennet-Clark 1977; Pollock and Shadwick 1994a). Similarly, in locust legs, the tibia (tool) can also account for some elastic energy storage (Bennet-Clark 1975; Katz and Gosline 1992, 1994). Although these blurred boundaries among the units may make our approach intractable in some systems, most power-amplified mechanisms do have discrete, quantifiable units that are amenable to these kinds of analyses.

In conclusion, this study has shown that a power-amplified structure can be divided into three functional units which belong to different developmental modules. If future studies reveal that other power-amplified systems are similarly modular, spatial matching between the different functional units and developmental modules in power-amplified systems raises a fundamental question: Did developmental modularity evolve first and subsequently lead to the evolution of an engine, an amplifier, and a tool, or do spatially localized selective pressures determine the different functional units and subsequently promote the evolution of modularity? Hopefully, our study will encourage future work on the comparative, macro-evolutionary biomechanics of power amplification mechanisms and lead to new insights into the origins and history of these remarkable systems.

ACKNOWLEDGMENTS

We particularly wish to thank E. Staaterman for assistance with animal sampling, maintenance, and force measurements. Thanks to M. Mendoza Blanco and T. Zack for help with strike force measurements, A. Stubbs with digitizing, T. F. Kosar for technical assistance with the micro-CT scans, M. L. Zelditch and D. L. Swiderski for their valuable advice on analysis, R. L. Caldwell for general advice and the Behavior and Morphology group of the Biology Department of the University of Massachusetts, Amherst for their constructive comments on the manuscript. The micro-CT scans were performed at the Center for Nanoscale Systems at Harvard University, a member of the National Nanotechnology Infrastructure Network (National Science Foundation award # ECS-0335765). This research was funded by a National Science Foundation Integrative Organismal Systems grant (#1014573 to S.N.P.) and by the University of California, Berkeley, Undergraduate Research Apprentice Program (to EC).

LITERATURE CITED

Ahyong, S. T. 2001. Revision of the Australian stomatopod crustacea. Australian Museum, Sydney.

Alexander, R. M. 1974. The mechanics of jumping by a dog (*Canis familiaris*). J. Zool. 173:549–573.

———. 1981. Factors of safety in the structure of animals. Sci. Prog. 67:109–130.

———. 1983. Animal mechanics. Blackwell Scientific Publications, Boston, MA.

Alexander, R. M., and H. C. Bennet-Clark. 1977. Storage of elastic strain energy in muscle and other tissues. Nature 265:114–117.

Alexander, R. M., A. S. Jayes, G. M. O. Maloiy, and E. M. Wathuta. 1981. Allometry of the leg muscles of mammals. J. Zool. 194:539–552.

Alexander, R. M., G. M. O. Maloiy, B. Hunter, A. S. Jayes, and C. N. Warui. 1982. The role of tendon elasticity in the locomotion of the camel (*Camelus dromedarius*). J. Zool. 198:293–313.

Allen, C. E. 2008. The "Eyespot Module" and eyespots as modules: development, evolution, and integration of a complex phenotype. J. Exp. Zool. Part B 310B:179–190.

Atchley, W. R., and B. K. Hall. 1991. A model for development and evolution of complex morphological structures. Biol. Rev. 66:101–157.

Atchley, W. R., A. A. Plummer, and B. Riska. 1985. Genetics of mandible form in the mouse. Genetics 111:555–577.

Barghusen, H. R. 1975. A review of fighting adaptations in dinocephalians (Reptilia, Therapsida). Paleobiology 1:295–311.

Barki, A., I. Karplus, and M. Goren. 1992. Effects of size and morphotype on dominance hierarchies and resource competition in the freshwater prawn *Macrobrachium rosenbergii*. Anim. Behav. 44:547–555.

Bennet-Clark, H. C. 1975. The energetics of the jump of the locust *Schistocerca gregaria*. J. Exp. Biol. 63:53–83.

Bennett, M. B., and G. C. Taylor. 1995. Scaling of elastic strain energy in kangaroos and the benefits of being big. Nature 378:56–59.

Biewener, A. A. 1989. Scaling body support in mammals: limb posture and muscle mechanics. Science 245:45–48.

Biewener, A. A., and R. Blickhan. 1988. Kangaroo rat locomotion: design for elastic energy storage or acceleration? J. Exp. Biol. 140:243–255.

Biewener, A. A., R. M. Alexander, and H. C. Heglund. 1981. Elastic energy storage in the hopping of kangaroo rats (*Dipodomys spectabilis*). J. Zool. 195:369–383.

Block, J. D., and S. Rebach. 1998. Correlates of claw strength in the rock crab, *Cancer irroratus* (Decapoda, Brachyura). Crustaceana 71:468–473.

Blundon, J. A. 1988. Morphology and muscle stress of chelae of temperate and tropical stone crabs *Menippe mercenaria*. J. Zool. 215:663–673.

Bolker, J. A. 2000. Modularity in development and why it matters to Evo-Devo. Am. Zool. 40:770–776.

Bookstein, F. L. 1991. Morphometric tools for landmark data, geometry and biology. Cambridge Univ. Press, Cambridge, MA.

———. 1997. Landmark methods for forms without landmarks: morphometrics of group differences in outline shape. Medical Image Analysis 1:225–243.

Borrell, B. J. 2004. Mechanical properties of calcified exoskeleton from the neotropical millipede, *Nyssodesmus python*. J. Insect Physiol. 50:1121–1126.

Browne, W. E., and N. H. Patel. 2000. Molecular genetics of crustacean feeding appendage development and diversification. Semin. Cell Dev. Biol. 11:427–435.

Burrows, M. 1969. The mechanics and neural control of the prey capture strike in the mantid shrimps *Squilla* and *Hemisquilla*. Zeitschrift für Vergleichende Physiologie 62:361–381.

Burrows, M., and G. Hoyle. 1972. Neuromuscular physiology of the strike mechanism of the mantis shrimps, *Hemisquilla*. J. Exp. Zool. 179:379–394.

Caldwell, R. L. 1975. Ecology and evolution of agonistic behavior in stomatopods. Naturwissenschaften 62:214–222.

Caldwell, R. L., and H. Dingle. 1976. Stomatopods. Scientific Am. 234:81–89.

Cheverud, J. M., S. E. Hartman, J. T. Richtsmeier, and W. R. Atchley. 1991. A quantitative genetic analysis of localized morphology in mandibles of inbred mice using finite-element scaling analysis. J. Craniofacial Genet. Dev. Biol. 11:122–137.

Choi, I. H., J. H. Shim, Y. S. Lee, and R. E. Ricklefs. 2000. Scaling of jumping performance in anuran amphibians. J. Herpetol. 34:222–227.

Claverie, T., and I. P. Smith. 2007. Functional significance of an unusual chela dimorphism in a marine decapod: specialization as a weapon? Proc. R. Soc. Lond. B 274:3033–3038.

———. 2009. Morphological maturity and allometric growth in the squat lobster *Munida rugosa*. J. Mar. Biol. Assoc. U.K. 89:1189–1194.

———. 2010. Allometry and sexual dimorphism in the chela shape in the squat lobster *Munida rugosa*. Aquat. Biol. 8:179–187.

Crane, J. 1975. Fiddler crabs of the world (Ocypodidae: genus *Uca*). Princeton Univ. Press, Princeton, NJ.

de Groot, J. H., and J. L. van Leeuwen. 2004. Evidence for elastic projection mechanism in the chameleon tongue. Proc. R. Soc. Lond. B 271:761–770.

Deban, S. M., J. C. O'Reilly, U. Dicke, and J. L. Van Leeuwen. 2007. Extremely high-power tongue projection in plethodontid salamanders. J. Exp. Biol. 210:655–667.

Dimery, N. J., and R. M. Alexander. 1985. Elastic properties of the hind foot of the donkey (*Equus asinus*). J. Zool. 207:9–20.

Dimery, N. J., R. F. Ker, and R. M. Alexander. 1986. Elastic properties of the feet of deer (Cervidae). J. Zool. 208:161–169.

Dryden, I. L., and K. V. Mardia. 1998. Statistical shape analysis. John Wiley & Sons, Chichester.

Edwards, D. 2000. Introduction to graphical modelling. Springer-Verlag, New York.

Edwards, J., D. Whitaker, S. Klionsky, and M. J. Laskowski. 2005. A record-breaking pollen catapult. Nature 435:164.

Ettema, G. J. C. 1996. Elastic and length-force characteristics of the gastrocnemius of the hopping mouse (*Notomys Alexis*) and the rat (*Rattus norvegicus*). J. Exp. Biol. 199:1277–1285.

Felsenstein, J. 1985. Phylogenies and the comparative method. Am. Nat. 125:1–15.

Gabbanini, F., F. Gherardi, and M. Vannini. 1995. Force and dominance in the agonistic behavior of the freshwater crab *Potamon fluviatile*. Aggressive Behav. 21:451–462.

Gronenberg, W. 1995a. The fast mandible strike in the trap-jaw ant *Odontomachus* II. Motor control. J. Comp. Physiol. A 176:399–408.

———. 1995b. The fast mandible strike on the trap-jaw ant *Odontomachus* I. Temporal properties and morphological characteristics. J. Comp. Physiol. A 176:391–398.

———. 1996. Fast actions in small animals: springs and click mechanisms. J. Comp. Physiol. A 178:727–734.

Gronenberg, W., and B. Ehmer. 1996. The mandible mechanism of the ant genus *Anochetus* (Hymenoptera, Formicidae) and the possible evolution of trap-jaws. Zoology 99:153–162.

Gronenberg, W., J. Tautz, and B. Hölldobler. 1993. Fast trap jaw and giant neurons in the ant *Odontomachus*. Science 262:561–563.

Hallgrímsson, B., K. Willmore, and B. K. Hall. 2002. Canalization, developmental stability, and morphological integration in primate limbs. Yearb. Phys. Anthropol. 45:131–158.

Hartnoll, R. G. 1974. Variation in growth pattern between some secondary sexual characters in crabs (Decapoda Brachyura). Crustaceana 27:131–136.

Herrel, A., J. J. Meyers, P. Aerts, and K. Nishikawa. 2000. The mechanics of prey prehension in chameleons. J. Exp. Biol. 203:3255–3263.

James, R. S., C. A. Navas, and A. Herrel. 2007. How important are skeletal muscle mechanics in setting limits on jumping performance? J. Exp. Biol. 210:923–933.

Katz, S. L., and J. M. Gosline. 1992. Ontogenetic scaling and mechanical behaviour of the tibiae of the African desert locust (*Schistocerca gregaria*). J. Exp. Biol. 168:125–150.

———. 1993. Ontogenetic scaling of jump performance in the African desert locust (*Shistocerca gregaria*). J. Exp. Biol. 177:81–111.

———. 1994. Scaling modulus as a degree of freedom in the design of locust legs. J. Exp. Biol. 187:207–223.

Klingenberg, C. P. 2008. Morphological integration and developmental modularity. Annu. Rev. Ecol. Evol. Syst. 39:115–132.

———. 2009. Morphometric integration and modularity in configurations of landmarks: tools for evaluating *a priori* hypotheses. Evol. Dev. 11:405–421.

Klingenberg, C. P., and G. S. McIntyre. 1998. Geometric morphometrics of developmental instability: analyzing patterns of fluctuating asymmetry with Procrustes methods. Evolution 52:1363–1375.

Klingenberg, C. P., and S. D. Zaklan. 2000. Morphological integration between developmental compartments in the *Drosophila* wing. Evolution 54:1273–1285.

Klingenberg, C. P., A. V. Badyaev, S. M. Sowry, and N. J. Beckwith. 2001. Inferring developmental modularity from morphological integration: analysis of individual variation and asymmetry in bumblebee wings. Am. Nat. 157:11–23.

Klingenberg, C. P., M. Barluenga, and A. Meyer. 2002. Shape analysis of symmetric structures: quantifying variation among individuals and asymmetry. Evolution 56:1909–1920.

Klingenberg, C. P., M. Katharina, and J. C. Auffray. 2003. Developmental integration in a complex morphological structure: how distinct are the modules in the mouse mandible? Evol. Dev. 5:522–531.

Lee, S. Y. 1993. Chela height is an acceptable indicator of chela strength in *Carcinus maenas* (Linnaeus, 1758) (Decapoda, Brachyura). Crustaceana 65:115–116.

Levinton, J. S., M. L. Judge, and J. P. Kurdziel. 1995. Functional differences between the major and the minor claws of fiddler crabs (*Uca*, family Ocypodidae, order Decapoda, subphylum Crustacea): a result of selection or developmental constraint? J. Exp. Mar. Biol. Ecol. 193:147–160.

Lundrigan, B. 1996. Morphology of horns and fighting behavior in the family Bovidae. J. Mammal. 77:462–475.

Magwene, P. M. 2001. New tools for studying integration and modularity. Evolution 55:1734–1745.

Marquez, E. 2008a. Coriandis: correlation analysis based on distances. Univ. of Michigan Museum of Zoology, MI.

———. 2008b. Sage: symmetry and asymmetry in geometric data. Univ. of Michigan Museum of Zoology, MI.

———. 2008c. A statistical framework for testing modularity in multidimensional data. Evolution 62:2688–2708.

McGowan, C. P., J. Skinner, and A. A. Biewener. 2008. Hind limb scaling of kangaroos and wallabies (superfamily Macropodoidea): implications for hopping performance, safety factor and elastic savings. J. Anat. 212:153–163.

Mezey, J. G., J. M. Cheverud, and G. P. Wagner. 2000. Is the genotype-phenotype map modular? A statistical approach using mouse quantitative trait loci data. Genetics 156:305–311.

Mitchell, S. C., S. M. Kennedy, P. J. Williams, and M. E. DeMont. 2003. Morphometrics and estimates of force generation by the chelae of a North American population of the invasive green crab, *Carcinus maenas* (L.). Can. J. Zool. 81:203–215.

Mitterœcker, P., and P. Gunz. 2009. Advances in geometric morphometrics. Evol. Biol. 36:235–247.

Moss, M. L. 1968. Functional cranial analysis of mammalian mandibular ramal morphology. Acta Anatomica 71:423.

Moss, M. L., and L. Salentijn. 1969. Primary role of functional matrices in facial growth. Am. J. Orthodontics 55:566–577.

Otto, S. P. 2004. Two steps forward, one step back: the pleiotropic effects of favoured alleles. Proc. R. Soc. Lond. B 271:705–714.

Palmer, A. R. 1996. Waltzing with asymmetry. Bioscience 46:518–532.

Palmer, A. R., and C. Strobeck. 1986. Fluctuating asymmetry: measurement, analysis, patterns. Ann. Rev. Ecol. Syst. 17:391–421.

Pangamiban, G., A. Sebring, L. Nagy, and S. Carroll. 1995. The development of crustacean limbs and the evolution of arthropods. Science 270:1363–1366.

Patek, S. N., and R. L. Caldwell. 2005. Extreme impact and cavitation forces of a biological hammer: strike forces of the peacock mantis shrimp *Odontodactylus scyllarus*. J. Exp. Biol. 208:3655–3664.

Patek, S. N., W. L. Korff, and R. L. Caldwell. 2004. Deadly strike mechanism of a mantis shrimp. Nature 428:819–820.

Patek, S. N., J. E. Baio, B. L. Fisher, and A. V. Suarez. 2006. Multifunctionality and mechanical origins: ballistic jaw propulsion in trap-jaw ants. Proc. Natl. Acad. Sci. USA 103:12787–12792.

Patek, S. N., B. N. Nowroozi, J. E. Baio, R. L. Caldwell, and A. P. Summers. 2007. Linkage mechanics and power amplification of the mantis shrimp's strike. J. Exp. Biol. 210:3677–3688.

Peterson, J. A., J. A. Benson, J. G. Morin, and M. J. McFall-Ngai. 1984. Scaling in tensile "skeletons": scale dependent length of the achilles tendon in mammals. J. Zool. 202:361–372.

Pit, J. H., and P. C. Southgate. 2003. Fouling and predation: how do they affect growth and survival of the blacklip pearl oyster, *Pinctada margaritifera*, during nursery culture? Aquac. Int. 11:545–555.

Pollock, C. M., and R. E. Shadwick. 1994a. Allometry of muscle, tendon, and elastic energy-storage capacity in mammals. Am. J. Physiol. 266:R1022–R1031.

———. 1994b. Relationship between body mass and biomechanical properties of limb tendons in adult mammals. Am. J. Physiol. 266:R1016–R1021.

R Development Core Team. 2009. R: a language and environment for statistical computing. R Foundation for Statistical Computing, Vienna, Austria.

Roberts, T. J., R. L. Marsh, P. G. Weyand, and C. R. Taylor. 1997. Muscular force in running turkeys: the economy of minimizing work. Science 275:1113–1115.

Rohlf, F. J. 2005a. TpsDig2, digitize landmarks and outlines. Department of Ecology and Evolution, State Univ. of New York at Stony Brook, Stony Brook, NY.

———. 2005b. TpsRelw, relative warps. Department of Ecology and Evolution, State Univ. of New York at Stony Brook, Stony Brook, NY.

Rohlf, F. J., and D. Slice. 1990. Extensions of the Procrustes method for the optimal superimposition of landmarks. Syst. Zool. 39:40–59.

Rothschild, M., Y. Schlein, K. Parker, and S. Sternberg. 1972. Jump of the oriental rat flea *Xenopsylla cheopis* (Roths.). Nature 239:45–48.

Schaffer, W. M. 1968. Intraspecific combat and the evolution of the *Caprini*. Evolution 22:817–825.

Schenk, S. C., and P. C. Wainwright. 2001. Dimorphism and the functional basis of claw strength in six brachyuran crabs. J. Zool. 255:105–119.

Schlosser, G. 2002. Modularity and the units of evolution. Theor. Biosci. 121:1–80.

Sheets, H. D. 2001. IMP: regress6. Department of Physics, Canisius College, Buffalo, NY.

———. 2006. IMP: Manovaboard 6.4. Department of Physics, Canisius College, Buffalo, NY.

Shuster, S. M., and R. L. Caldwell. 1989. Male defense of the breeding cavity and factors affecting the persistence of breeding pairs in the stomatopod, *Gonodacylus bredini* (Manning) (Crustacea: Hoplocarida). Ethology 82:192–207.

Sneddon, L. U., F. A. Huntingford, and A. C. Taylor. 1997. Weapon size versus body size as a predictor of winning in fights between shore crabs, *Carcinus maenas* (L.). Behav. Ecol. Sociobiol. 41:237–242.

Sneddon, L. U., F. A. Huntingford, A. C. Taylor, and J. F. Orr. 2000. Weapon strength and competitive success in the fights of shore crabs (*Carcinus maenas*). J. Zool. 250:397–403.

Snell-Rood, E. C., J. D. Van Dyken, T. Cruickshank, M. J. Wade, and A. P. Moczek. 2010. Toward a population genetic framework of developmental evolution: the cost, limits, and consequences of phenotypic plasticity. Bioessays 32:71–81.

Snively, E., and A. Cox. 2008. Structural mechanics of pachycephalosaur crania permitted head-butting behavior. Palaeo Electronica 11:1–17.

Spagna, J. C., A. I. Vakis, C. A. Schmidt, S. N. Patek, X. Zhang, N. D. Tsutsui, and A. V. Suarez. 2008. Phylogeny, scaling, and the generation of extreme forces in trap-jaw ants. J. Exp. Biol. 211:2358–2368.

Stein, R. A. 1976. Sexual dimorphism in crayfish chelae: functional significance linked to reproductive activities. Can. J. Zool. 54:220–227.

Taylor, G. M. 2001. The evolution of armament strength: evidence for a constraint on the biting performance of claws of durophagous decapods. Evolution 55:550–560.

Van Wassenbergh, S., J. A. Strother, B. E. Flammang, L. A. Ferry-Graham, and P. Aerts. 2008. Extremely fast prey capture in pipefish is powered by elastic recoil. J. R. Soc. Interface 5:285–296.

Wagner, G., and L. Altenberg. 1996. Perspective: complex adaptations and the evolution of evolvability. Evolution 50:967–976.

Wagner, G. P. 1996. Homologues, natural kinds and the evolution of modularity. Am. Zool. 36:36–43.

Waxman, D., and J. R. Peck. 1998. Pleiotropy and the preservation of perfection. Science 279:1210–1213.

West-Eberhard, M. J. 2003. Developmental plasticity and evolution. Oxford Univ. Press, New York NY.

Williams, S. B., R. C. Payne, and A. M. Wilson. 2007. Functional specialisation of the pelvic limb of the hare (*Lepus europeus*). J. Anat. 210:472–490.

Williams, T. A., and L. M. Nagy. 2001. Developmental modularity and the evolutionary diversification of arthropod limbs. J. Exp. Zool. 291:241–257.

Wilson, R. S., C. E. Franklin, and R. S. James. 2000. Allometric scaling relationships of jumping performance in the striped marsh frog *Limnodynastes peronii*. J. Exp. Biol. 203:1937–1946.

Young, N. M., and B. Hallgrimsson. 2005. Serial homology and the evolution of mammalian limb covariation structure. Evolution 59:2691–2704.

Zack, T. I., T. Claverie, and S. N. Patek. 2009. Elastic energy storage in the mantis shrimp's fast predatory strike. J. Exp. Biol. 212:4002–4009.

Zelditch, M. L., D. L. Swiderski, H. D. Sheets, and W. L. Fink. 2004. Geometric morphometrics for biologists: a primer. Elsevier Academic Press, New York.

Zelditch, M. L., A. R. Wood, and D. L. Swiderski. 2009. Building developmental integration into functional systems: function-induced integration of mandibular shape. Evol. Biol. 36:71–87.

Associate Editor: R. Dudley